SEMARAK ILMU PUBLISHING

Journal of Advanced Research in Fluid Mechanics and Thermal Sciences

Journal homepage:
https://semarakilmu.com.my/journals/index.php/fluid_mechanics_thermal_sciences/index
ISSN: 2289-7879

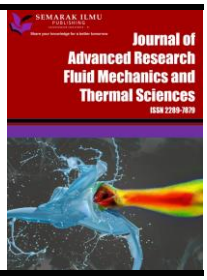

A Study of Soret-Dufour Effects on MHD Radiative Casson Nanofluid Flow Past an Inclined Surface with Chemical Reaction

Giulio Lorenzini[1,*], Prathi Vijaya Kumar[2], Shaik Mohammed Ibrahim[3]

[1] Department of Engineering and Architecture, University of Parma, Parco Area delle Scienze, 181/A, Parma 43124, Italy
[2] Department of Mathematics, GITAM (Deemed to be University), Visakhapatnam, Andhra Pradesh 530045, India
[3] Department of Mathematics, Koneru Lakshmaiah Education Foundation, Green Fileds, Vaddeswaram, Andhra Pradesh. – 522302, India

ARTICLE INFO

Article history:
Received 8 September 2023
Received in revised form 23 November 2023
Accepted 2 December 2023
Available online 15 December 2023

Keywords:
Casson nanofluid; inclination surface; Soret; Dufour; HAM

ABSTRACT

This study investigates the impact of heat flux induced by concentration gradients (Dufour effects) and temperature gradients (Soret effects) on the boundary layer flow of a Casson nanofluid over an inclined expanding surface. It also considers heat and mass transfer coupled processes, Brownian motion, thermal radiation, chemical reactions, and thermophoresis. A dimensionless problem is formulated using similarity transformations and solved using the homotopy analysis method (HAM). Tables and graphs are employed to illustrate the correlations between influencing factors and physical quantities. It is observed that an increase in the inclination parameter leads to a reduction in skin friction but an enhancement in Nusselt and Sherwood numbers. The inclination parameter causes a decline in velocity, while the opposite trend is observed in the concentration field for the chemical reaction parameter. The Casson parameter decelerates the velocity and accelerates the distributions of temperature and concentration. The findings provide valuable insights into the flow patterns, temperature distribution, and concentration profiles within the system. This information holds significant relevance for designing and optimizing heat transfer systems, energy-efficient processes, and catalytic reactors involving Casson nanofluids. Our claims are validated by comparison with published literature, demonstrating a high degree of agreement.

1. Introduction

In a fluid flow and thermal analysis, traditional fluids like oil, water, glycol, etc., have a lower performance of heat transfer and low thermal conductivity. To find the innovations and research to enrich the thermal conductivity and heat transfer by using the metallic or nonmetallic additives with high thermal conductivity, nano-sized tiny particles called nanoparticles add in a base/pedestal fluid. This fluid dispersion of nanoparticles is called nanofluid. Nanofluid plays a significant role due to its wide range of applications in electronic and engine cooling, medical science, textile manufacturing, nuclear reactor, microelectronics, power saving, etc. Nanofluid has a better heat transfer rate due to

* *Corresponding author.*
E-mail address: giulio.lorenzini@unipr.it

https://doi.org/10.37934/arfmts.112.1.217235

improved thermal conductivity by these nanoparticles. This type of new technology is very useful for development specially to make better lubricants and oil. This novel concept of nano-fluid was originally developed by Choi and Eastman [1]. In the early 21st century, this new type of nanofluid had a huge impact, attracting researchers to do more work on heat transfer analysis in various fields. Nakhchi and Esfahani [2] investigated the numerical solution of turbulent flow in copper-water nanofluids passing through heat exchanger tubes with conical rings of holes. Using the finite element method for different Reynolds numbers, they found that heat transfer was significantly enhanced. They found that heat transfer was significantly enhanced. Ambreen *et al.,* [3] analyzed the properties of nanofluid-cooled micro-pin fins and water by implementing a two-phase model of the Euler-Langrangian method to simplify fluid flow under constant pressure and a heat sink. They investigated the effect of adding nanometer-sized particles to the fluid on heat transfer. Borah *et al.,* [4] studied conjugate heat transfer in pipes with fixed wall thickness and non-uniform heat sources using the formulation of the two-phase model of the Euler-Langrangian method. They investigated the damping effect and found that heat transfer in nanofluids is reduced due to inhomogeneous heat sources. Javaherdeh *et al.,* [5] analyzed the enrichment of laminar heat transfer for non-Newtonian fluids in parallel channels partially filled with porous media by employing the Darcy model, elucidating that developing in Reynolds number enhances the transfer of heat. Waqas *et al.,* [6] deliberated the fluid motion and transfer of heat of nano fluid through a stretching porous cylinder with viscous dissipation and thermal radiation. Jha and Aina [7] presented the influences of temperature jump and slip conditions for established MHD-driven natural convection flow of viscous, fluid in the vertical microporous channel designed by an electrically non-conducting unbounded plate in the existence of an induced magnetic field. Elsaid and Abdel-wahed [8] studied and solved numerically the mixed convection of Ferro hybrid nano fluid through a perpendicular channel in the presence of a constant transverse magnetic field with thermal radiation and variable temperature. Iqbal *et al.,* [9] analyzed the unsteady MHD nano fluid motion in a rotating channel with the effects of hall current and thermal radiation. Alharbi [10] studied and detected the characteristics of the laminar flow of nanofluid motion and transfer of heat to a permeable plate in magnetic induction with radiation effect which contributes to the cooling process of devices. Rheological behaviour and experimental study on hybrid nanofluids have been studied Sharma *et al.,* [11].

Many researchers have focused on the concept of Casson fluid as they have gigantic applications in fields like polymer processing, biomechanics, drilling operations, metallurgy, etc. Casson fluid constitutive equation delineate a nonlinear relationship among stress and rate of strain and has been observed to be perfectly admissible to silicon suspensions, suspensions of bentonite in water, and lithographic varnishes used for printing inks. Casson fluid is a shear-thinning fluid that is supposed to have an infinite viscosity at zero shear rate, yield stress below which there is no flow and zero viscosity at an infinite shear rate. This means that if the shear stress is lower than the yield stress, it acts like a solid. However, Casson fluid tends to flow as the shear stress exceeds the yield stress. Some examples of Casson fluid are Jelly, salt solutions, ketchup, paints, shampoo, tomato sauce, honey, soup, concentrated fruit juices, and so on. Mintsa *et al.,* [12] observed the effects of a magnetic field and an electrically conductive of an incompressible Casson nanofluid on heat and mass transfer through an accelerated stretched plate considering the nanofluid. Rafique *et al.,* [13] explored the Soret and Dufour effects on Casson nanofluid flow using Keller box method, a numerical method for solving partial differential equations. Mukhopadhyay [14] reported that the Casson parameter depreciates the velocity field. Mustafa and Khan [15] discussed the magnetic field effect on Casson nanofluid over a nonlinearly stretched sheet. Gnanaprasanna and Singh [16] studied the rheological properties of Casson nanofluids flowing on a vertical plate. Hayat *et al.,* [17] studied the Soret and Dufour effects on the magnetohydrodynamic (MHD) flow of the Casson fluid over a

stretched surface. Later various aspects of this problem have been studied by many researchers [18-24].

The study of the boundary layer flow, heat and mass transfer is important due to its many applications in industries and many manufacturing processes such as aerodynamic extrusion of plastic sheets and cooling of metallic sheets in a cooling bath. During its manufacturing process a stretched sheet interacts with ambient fluid thermally and mechanically. Prasad *et al.,* [25] discussed and analysed the diffusion thermo and chemical reaction effects on the free convection heat and mass transfer flow of nanofluid over a vertical plate embedded in a porous medium in the presence of radiation absorption and a constant heat source. Akbar *et al.,* [26] presented the numerical study of heat and mass transfer analysis in a viscous unsteady MHD nanofluid flow. The steady boundary layer flow of nanofluid over an exponential stretching surface is investigated analytically by Nadeem and Lee [27]. The significance of thin fluid flow along an inclined plate in various physical and engineering contexts has come to be recognized in recent years, leading to increased research on the subject. These insights are essential because they will advance our theoretical and practical understanding of a variety of thin film-related situations that arise in the real world. Examples include heat exchangers, lubrication, electroplating, and the flow of fluid in connective tissue. Thin film flow analysis across a heated inclined plane was therefore proposed by Kay *et al.,* [28] based on environmental model data. Srinivasulu and Bandari [29] deliberated the impact of non-linear thermal radiation and non-uniform heat source/sink on MHD boundary layer flow of Williamson nanofluid above an inclined stretching surface. Heat transfer of MHD flow over an inclined past stretching sheet is studied by Ali *et al.,* [30]. Ramesh *et al.,* [31] studied dust boundary layer flow of MHD fluid and heat transfer over an inclined stretching sheet with non-uniform heat source/sink. Nandeppanavar *et al.,* [32] discussed the flow, heat and mass transfer of MHD Casson nanofluid due to an inclined stretching sheet. Rafique and Alotaibi [33] discussed the effects of heat generation/absorption and chemical reaction on magnetohydrodynamics (MHD) flow of non-Newtonian nanofluid over an inclined stretching surface. Nanofluid flow under the magnetic field effects over an inclined stretching sheet has been worked out by Shah *et al.,* [34]. Saeed *et al.,* [35] investigate the influences and features of magnetohydrodynamic thermophoresis and brownian motion of unsteady 2D non-linear convective flow of thin film nanofluid over an inclined stretching sheet. Because most nonlinear differential equations do not have analytical solutions, approximation and numerical approaches are frequently used. Because many nonlinear equations do not have a small parameter, all classical perturbation techniques require it, which restricts the use of all traditional perturbation methods. The determination of a small parameter is a difficult operation that necessitates the employment of special techniques. The homotopy analysis method (HAM) is a semi-analytical technique that can be used to solve a wide range of nonlinear problems, including differential equations, integral equations, and boundary value problems. It is a powerful and versatile method that has been successfully applied to a variety of engineering and scientific problems. HAM has also been used to solve a variety of problems in other fields, such as electromagnetics, acoustics, and biology. For example, HAM has been used to study the propagation of electromagnetic waves, the sound waves in fluids and solids, and the diffusion of chemicals in biological systems. Many authors have employed HAM to overcome these challenges [36-40].

Four novel aspects served as the basis for our current effort. The primary goal of this study was to simulate and analyze the Casson nanofluid flow over a nonlinear inclined stretching surface. The second objective is to examine the dynamics of this flow over an inclined surface. The third step is to examine characteristics of the thermal radiation, chemical reaction, Soret effect, Brownian motion, and thermophoresis. As a fourth goal, we intend to use the HAM method to generate numerical solutions for the velocity, temperature, and concentration fields. Also, graphical analyses of the skin

friction coefficient and the local Nusselt and Sherwood numbers have been performed. To our knowledge, the problem is new and no such articles reported yet in the literature.

2. Mathematical Formulation

In this study, we have considered a transfer of non-Newtonian fluid (Casson) nanofluid via 2D boundary layer flow over a non(linear), expanding surface with an inclined angle Ω. Being a valid coordinate along the presumed constancy of the expanding surface, and 'a' is the assumed constant, we take it that the continuing and free stream velocities are $u_w(x) = ax^m$ and $u_\infty(x) = 0$, respectively. The magnetic field $B_0(x)$ is a transverse external field, perpendicular to the direction of the flow. The effects of chemical reactions, heat radiation, and the Soret/Dufour impacts are all considered. Figure 1, illustrates the constant values T_w and C_w for the wall temperature T and nanoparticle fraction C, respectively, whereas the ambient forms C_∞ and T_∞ for the nanofluid mass and temperature fraction are achieved as approximations to infinity. The Joule heating term is omitted from the energy equation when the electrical conductivity of the fluid is low or when the electric field is weak. In these cases, the heat generated by Joule heating is negligible and can be omitted from the energy equation without introducing a significant error.

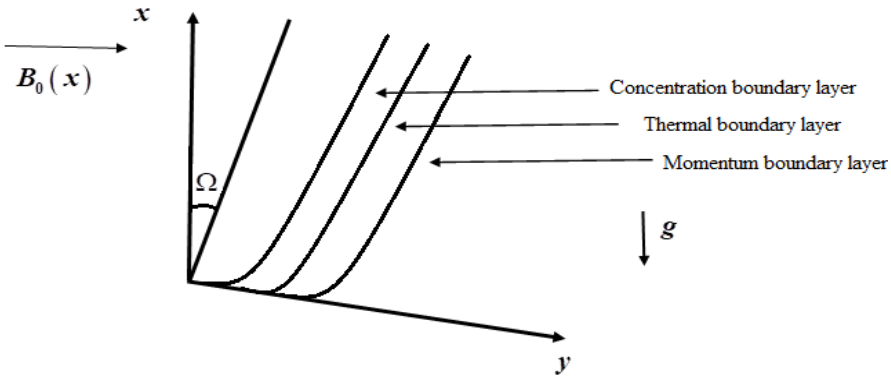

Fig. 1. Related schematic flow of the model

The mentioned problem is governed by the following equations.

$$\frac{\partial u}{\partial x} + \frac{\partial v}{\partial y} = 0, \tag{1}$$

$$u\frac{\partial u}{\partial x} + v\frac{\partial u}{\partial y} = \nu\left(1 + \frac{1}{\beta}\right)\frac{\partial^2 u}{\partial y^2} + g\left[\beta_t\left(T - T_\infty\right) + \beta_c\left(C - C_\infty\right)\right]\cos\Omega - \frac{\sigma B_0^2(x)u}{\rho_f}, \tag{2}$$

$$u\frac{\partial T}{\partial x} + v\frac{\partial T}{\partial y} = \alpha\frac{\partial^2 T}{\partial y^2} - \frac{1}{(\rho C)_f}\frac{\partial q_r}{\partial y} + \tau\left[D_B\frac{\partial C}{\partial y}\frac{\partial T}{\partial y} + \frac{D_T}{T_\infty}\left(\frac{\partial T}{\partial y}\right)^2\right] + \frac{D_T K_T}{C_s C_p}\frac{\partial^2 C}{\partial y^2}, \tag{3}$$

$$u\frac{\partial C}{\partial x} + v\frac{\partial C}{\partial y} = D_B\frac{\partial^2 C}{\partial y^2} + \frac{D_T K_T}{T_\infty}\frac{\partial^2 T}{\partial y^2} - Kr\left(C - C_\infty\right), \tag{4}$$

Using the Rosseland's approximation for radiation, the radiation heat flux is simplified as [34,35]

$$q_r = -\frac{4\sigma^*}{3k^*}\frac{\partial T^4}{\partial y}. \tag{5}$$

In the above system of equations, σ^* (Stefan-Boltzmann constant), k^* (mean absorption factor). It is presumed that the temperature variance concerning the free steam T_∞ and local temperature T is insignificant adequate, escalating T^4 in Taylor series approximately T_∞ and ignoring greater order terms for:

$$T^4 \cong 4T_\infty^3 T - 3T_\infty^4, \tag{6}$$

The remedy to Eq. (3) can be derived from Eq. (5) and Eq. (6) as follows:

$$u\frac{\partial T}{\partial x} + v\frac{\partial T}{\partial y} = \left(\alpha + \frac{16\sigma^*}{3k^*(\rho C)_f}\right)\frac{\partial^2 T}{\partial y^2} + \tau\left[D_B\frac{\partial C}{\partial y}\frac{\partial T}{\partial y} + \frac{D_T}{T_\infty}\left(\frac{\partial T}{\partial y}\right)^2\right] + \frac{D_T K_T}{C_s C_p}\frac{\partial^2 C}{\partial y^2}, \tag{7}$$

In which *u, v* (velocity constituents in the x and y directions), g (acceleration due to gravity), B_0 (uniform magnetic field strength), σ (electrical conductivity), μ (dynamic viscosity), ρ_f (density of the base fluid), ρ_p (density of the nanoparticle), β (Casson parameter), β_t (factor of thermal expansion), β_c (quantity of concentration expansion), D_B (Brownian diffusion factor), D_T (thermophoresis diffusion factor), k (thermal conductivity), $(\rho C)_p$ (heat capacitance of the nanoparticles), $(\rho C)_f$ (heat capacitance of the base fluid), $\alpha = \frac{k}{(\rho C)_f}$ (thermal diffusivity parameter), $\tau = \frac{(\rho C)_p}{(\rho C)_f}$ (fraction between the effective heat capacity of the nanoparticle and heat capacity of the fluid), and Kr (chemical reaction parameter).

The corresponding BCs are:

$$\begin{aligned} &u = u_w(x) = ax^m, v = 0, T = T_w, C = C_w, aty = 0 \\ &u \to u_\infty(x) = 0, v \to 0, T \to T_\infty, C \to C_\infty aty \to \infty, \end{aligned} \tag{8}$$

The stream function $\psi = \psi(x, y)$ is defined as:

$$u = \frac{\partial \psi}{\partial y}, v = -\frac{\partial \psi}{\partial x}, \tag{9}$$

For the above stream function, Eq. (1) is identically satisfied. The association conversions are defined as [13]:

$$\zeta = y\sqrt{\frac{(m+1)ax^{m-1}}{2v}}, \psi = \sqrt{\frac{2vax^{m+1}}{m+1}} f(\zeta), \theta(\zeta) = \frac{T-T_\infty}{T_w-T_\infty}$$
$$\phi(\zeta) = \frac{C-C_\infty}{C_w-C_\infty}, \tag{10}$$

The obtained dimensionless ordinary differential equations

$$\left(1+\frac{1}{\beta}\right) f''' + ff'' - \frac{2m}{m+1} f'^2 + \frac{2}{m+1}(\lambda\theta - \delta\phi)\cos\Omega - \left(\frac{2M}{m+1}\right) f' = 0 \tag{11}$$

$$\left(1+\frac{4}{3}R\right)\theta'' + \Pr f\theta' + \Pr Nb\phi'\theta' + \Pr Nt\,\theta'^2 + D_f\phi'' = 0, \tag{12}$$

$$\phi'' + \Pr Le\left(f\phi' + Sr\theta'' - \frac{2}{m+1}\gamma\phi\right) = 0 \tag{13}$$

where,

$$\lambda = \frac{Gr_x}{\mathrm{Re}}, \delta = \frac{Gc_x}{\mathrm{Re}}, M = \frac{\sigma B_0^2(x)}{\rho a}, Le = \frac{v}{D_B}, \Pr = \frac{v}{\alpha}, Nb = \frac{\tau D_B(C_w-C_\infty)}{v},$$
$$Nt = \frac{\tau D_t(T_w-T_\infty)}{vT_\infty}, Gr_x = \frac{g\beta_t(T_w-T_\infty)x}{av}, \mathrm{Re} = \frac{u_w x}{v}, Gc_x = \frac{g\beta_c(C_w-C_\infty)x}{av},$$
$$R = \frac{4\sigma^* T_\infty^3}{\alpha k^*}, D_f = \frac{D_T K_T(C_w-C_\infty)}{vC_s C_p(T_w-T_\infty)}, Sr = \frac{D_T K_T(T_w-T_\infty)}{vT_\infty(C_w-C_\infty)}, \gamma = \frac{Kr}{ax^{\frac{m-1}{2}}(C_w-C_\infty)}$$

Here, primes denote the differentiation with respect to ζ, Dufour number *(Du)*, radiation parameter (R), Buoyancy parameter (λ),Brownian motion parameter (*Nb*), *)*, chemical reaction parameter (γ), Solutal buoyancy parameter (δ),Prandtl number (*Pr*), magnetic parameter called Hartmann number (M), kinematic viscosity of the fluid (v),thermophoresis parameter (*Nt*), Soret number *(Sr*), Lewis number (*Le*).

The similarity transformations lead to the following conversion of boundary restrictions.

$$\phi(\zeta)=1, \quad \theta(\zeta)=1, \quad f'(\zeta)=1, \quad f(\zeta)=0 \quad at \quad \zeta=0,$$
$$\phi(\zeta)\to 0, \quad \theta(\zeta)\to 0, \quad f'(\zeta)\to 0 \; as \quad \zeta\to\infty, \tag{14}$$

2.1 Parameters of Empirical Importance

Local Skin-friction coefficients, local Nusselt number and local Sherwood number for the present problem are maintained as

$$C_f = \frac{\tau_w}{\rho u_w^2 \rho_f},\ Nu_x = \frac{xq_w}{k(T_w - T_\infty)},\ Sh_x = \frac{xq_m}{D_B(C_w - C_\infty)}\ ,$$

$$q_w = -k\frac{\partial T}{\partial y}, q_m = -D_B\frac{\partial C}{\partial y}, \tau_w = \mu\left(1+\frac{1}{\beta}\right)\frac{\partial u}{\partial y} at\ y = 0$$

Here, $\mathrm{Re}_x = \frac{u_w x}{\nu}$ (local Reynolds number) the above expressions in dimensionless form take the expressions as

$$-\theta'(0) = \frac{Nu_x}{\left(1+\frac{4}{3}N\right)\sqrt{\frac{m+1}{2}\mathrm{Re}}}, -\phi'(0) = \frac{Sh_x}{\sqrt{\frac{m+1}{2}\mathrm{Re}}}, \left(1+\frac{1}{\beta}\right) f''(0) = C_f\sqrt{\frac{2}{m+1}\mathrm{Re}}$$

3. HAM

Homotopic solutions of Eq. (11) to Eq. (14) are obtained by selecting the initial guesses and linear operators as follows.

$$f_0(\zeta) = \left(1+(-e^{-\zeta})\right),$$
$$\theta_0(\zeta) = e^{-\zeta},$$
$$\phi_0(\zeta) = e^{-\zeta}.$$

$$L_1(f) = f''' - f',$$
$$L_2(\theta) = \theta'' - \theta,$$
$$L_3(\phi) = \phi'' - \phi,$$

with

$$L_1\left(C_1 + C_2 e^{\zeta} + C_3 e^{-\zeta}\right) = 0,$$
$$L_2\left(C_4 e^{\zeta} + C_5 e^{-\zeta}\right) = 0,$$
$$L_3\left(C_6 e^{\zeta} + C_7 e^{-\zeta}\right) = 0,$$

where $C_i\,(i = 1 \text{ to } 7)$ are the arbitrary constants.

We construct the zeroth-order deformation equations

$$(1-p)\,L_1\left(f(\zeta;p) - f_0(\zeta)\right) = p\hbar_1 N_1\left[f(\zeta;p), \theta(\zeta;p), \phi(\zeta;p)\right], \tag{15}$$

$$(1-p)L_2\left(\theta(\zeta;p) - \theta_0(\zeta)\right) = p\hbar_2 N_2\left[f(\zeta;p), \theta(\zeta;p), \phi(\zeta;p)\right], \tag{16}$$

$$(1-p)L_3\left(\phi(\zeta;p)-\phi_0(\zeta)\right)=p\hbar_3 N_3\left[f(\zeta;p),\theta(\zeta;p),\phi(\zeta;p)\right], \tag{17}$$

subject to the boundary conditions

$$\begin{aligned} &f(0;p)=0, && f'(0;p)=1, && f'(\infty;p)=0,\\ &\theta(0;p)=1, && && \theta(\infty;p)=0,\\ &\phi(0;p)=1, && && \phi(\infty;p)=0, \end{aligned} \tag{18}$$

$$\begin{aligned} &N_1\left[f(\zeta;p),\theta(\zeta;p),\phi(\zeta,p)\right]=\left(1+\frac{1}{\beta}\right)f'''(\zeta;p)+f(\zeta;p)f''(\zeta;p)\\ &-\frac{2m}{m+1}\left(f'(\zeta;p)\right)^2+\frac{2}{m+1}\left(\lambda\theta(\zeta;p)-\delta\phi(\zeta;p)\right)\cos\Omega-\frac{2M}{m+1}f'(\zeta;p), \end{aligned} \tag{19}$$

$$\begin{aligned} &N_2\left[f(\zeta;p),\theta(\zeta;p),\phi(\zeta;p)\right]=\frac{1}{\Pr}\left(1+\frac{4}{3}R\right)\frac{\partial^2\theta(\zeta;p)}{\partial\zeta^2}\\ &+\left(f(\zeta;p)\frac{\partial\theta(\zeta;p)}{\partial\zeta}\right)+Nb\frac{\partial\theta(\zeta;p)}{\partial\zeta}\frac{\partial\phi(\zeta;p)}{\partial\zeta}+Nt\left(\frac{\partial\theta(\zeta;p)}{\partial\zeta}\right)^2+D_f\frac{\partial^2\phi(\zeta;p)}{\partial\zeta^2}, \end{aligned} \tag{20}$$

$$\begin{aligned} &N_3\left[f(\zeta;p),\theta(\zeta;p),\phi(\zeta;p)\right]=\frac{\partial^2\phi(\zeta;p)}{\partial\zeta^2}+Le\Pr\left(f(\zeta;p)\frac{\partial\phi(\zeta;p)}{\partial\zeta}-\frac{2}{m+1}\gamma\phi\right)\\ &+\Pr Le\,Sr\frac{\partial^2\theta(\zeta;p)}{\partial\zeta^2}, \end{aligned} \tag{21}$$

When p = 0 and p = 1, we obtain

$$\begin{aligned} &f(\zeta;0)=f_0(\zeta) && f(\zeta;1)=f(\zeta),\\ &\theta(\zeta;0)=\theta_0(\zeta) && \theta(\zeta;1)=\theta(\zeta),\\ &\phi(\zeta;0)=\phi_0(\zeta) && \phi(\zeta;1)=\phi(\zeta). \end{aligned} \tag{22}$$

Thus, as p varies from Zero (0) to one (1) then $f(\zeta;p)$, $\theta(\zeta;p)$ and $\phi(\zeta;p)$ changes from initial estimates to the accurate results of the unique nonlinear differential equations.

Utilizing Taylor's series, we understand

$$f(\zeta;p)=f_0(\zeta)+\sum_{n=1}^{\infty}f_n(\zeta)p^n, \tag{23}$$

$$\theta(\zeta;p)=\theta_0(\zeta)+\sum_{n=1}^{\infty}\theta_n(\zeta)p^n, \tag{24}$$

$$\phi(\zeta;p)=\phi_0(\zeta)+\sum_{n=1}^{\infty}\phi_n(\zeta)p^n, \tag{25}$$

where

$$f_n(\zeta)=\frac{1}{n!}\frac{\partial^n f(\zeta;p)}{\partial p^n}\bigg|_{p=0},$$
$$\theta_n(\zeta)=\frac{1}{n!}\frac{\partial^n \theta(\zeta;p)}{\partial p^n}\bigg|_{p=0}, \quad (26)$$
$$\phi_n(\zeta)=\frac{1}{n!}\frac{\partial^n \phi(\zeta;p)}{\partial p^n}\bigg|_{p=0}.$$

For the series (22) to (24), convergence can be guaranteed if the starting approximations, auxiliary linear operators, and non-zero auxiliary parameters are selected suitably.

$$f(\zeta)=f_0(\zeta)+\sum_{n=1}^{\infty} f_n(\zeta), \quad (27)$$

$$\theta(\zeta)=\theta_0(\zeta)+\sum_{n=1}^{\infty}\theta_n(\zeta), \quad (28)$$

$$\phi(\zeta)=\phi_0(\zeta)+\sum_{n=1}^{\infty}\phi_n(\zeta). \quad (29)$$

m[th]-charge distortion equations are as observes

$$L_1\left(f_n(\zeta)-\chi_n\, f_{n-1}(\zeta)\right)=\hbar_1 R_n^f(\zeta), \quad (30)$$

$$L_2\left(\theta_n(\zeta)-\chi_n\,\theta_{n-1}(\zeta)\right)=\hbar_2 R_n^\theta(\zeta), \quad (31)$$

$$L_3\left(\phi_n(\zeta)-\chi_n\,\phi_{n-1}(\zeta)\right)=\hbar_3 R_n^\phi(\zeta), \quad (32)$$

with the following boundary conditions

$$\begin{aligned} &f_n(0)=0, \qquad f_n'(0)=0, \quad f_n'(\infty)=0,\\ &\theta_n'(0)=0, \qquad\qquad \theta_n(\infty)=0,\\ &\phi_n(0)=0, \qquad\qquad \phi_n(\infty)=0, \end{aligned} \quad (33)$$

where

$$R_n^f(\zeta)=\left(1+\frac{1}{\beta}\right)f_{n-1}'''+\sum_{i=0}^{n-1} f_{n-1-i}\,f_i''-\frac{2m}{m+1}\sum_{i=0}^{n-1} f_{n-1-i}'\,f_i'+\frac{2m}{m+1}\left(\lambda\theta_{n-1}-\delta\,\phi_{n-1}\right)\cos\Omega$$
$$-\frac{2M}{m+1}f_{n-1}', \quad (34)$$

$$R_n^{\theta}(\zeta)=\frac{1}{\Pr}\left(1+\frac{4R}{3}\right)\theta_{n-1}^{''}+\sum_{i=0}^{n-1} f_{n-1-i}\,\theta_i^{'}+Nb\sum_{i=0}^{n-1}\theta'_{n-1-i}\,\phi_i^{'}+Nt\sum_{i=0}^{n-1}\theta'_{n-1-i}\,\theta_i^{'}-\Pr D_f\,\phi_{n-1}^{''}, \tag{35}$$

$$R_n^{\phi}(\zeta)=\phi_{n-1}^{''}+Le\Pr\left(\sum_{i=0}^{n-1} f_{n-1-i}\,\phi_i^{'}-\gamma\phi_{n-1}\right)+\Pr Sr\;Le\;\theta_{n-1}^{''}, \tag{36}$$

$$\chi_m=\begin{cases}0, & m\le 1,\\ 1, & m>1.\end{cases} \tag{37}$$

3.1 Convergence of HAM Solution

$\hbar_1,\hbar_2$ and $\hbar_3$. To acquire the relevant values for these parameters, $\hbar$-curves are portrayed in Figure 2. From the figure, it is scrutinized that the plausible region of the parameters is about $[-1.0,0.0]$. For $\hbar_1=\hbar_2=\hbar_3=-0.45$, the series solutions are convergent in the whole region of ζ . Table 1 displays the convergence of the method.

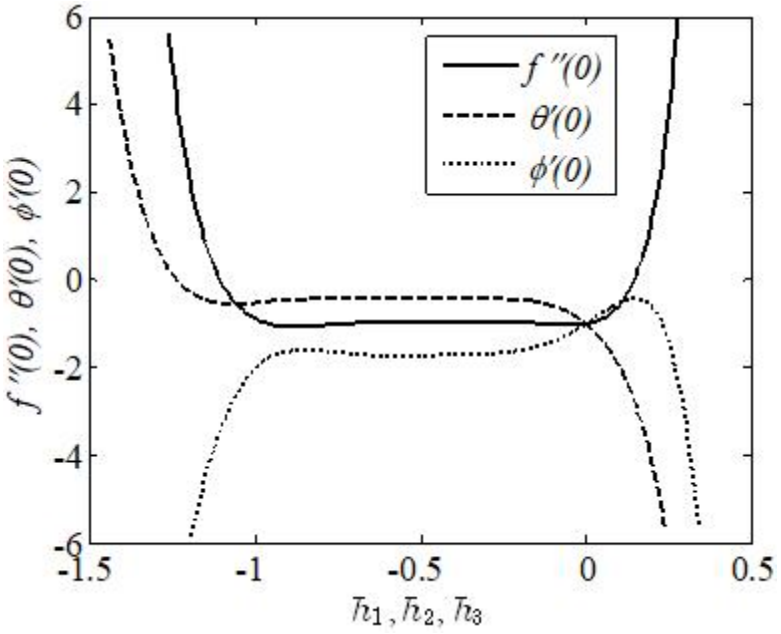

Fig. 2. $f''(0)$ $\theta'(0)$ and $\phi'(0)$ - $\hbar$-curves

Table 1
Order of approximation at which the HAM solutions converge when $\beta = 1.0, M = m = 0.5, \lambda = R = Sr = D_f = 0.1, \delta = 0.9, \Pr = Le = 2.0, Nb = Nt = 0.2, \gamma = 0.2, \Omega = \pi / 4.$

Order	$-f''(0)$	$-\theta'(0)$	$-\phi'(0)$
5	0.979147	0.384462	1.79158
10	0.979211	0.381463	1.792136
15	0.979220	0.381102	1.792081
20	0.979218	0.381058	1.792086
25	0.979218	0.381051	1.792087
30	0.979218	0.381050	1.792087
35	0.979218	0.381050	1.792087
40	0.979218	0.381050	1.792087
45	0.979218	0.381050	1.792087

4. Validation of the Work

Values of $-\theta'(0)$ and $\phi'(0)$ for different ranges of Nb and Nt are determined and compared to formerly existing work in Table 2. Comparison of the values of $-\theta'(0)$ with the existing results of Srinivasulu and Bandari [29] has been given in Table 3. The current outcomes are observed to be in limiting sense agreement with the preceding results.

Table 2
Assessment of $-\theta'(0)$ for different estimates of Nb and Nt when $M = R = \lambda = \delta = Sr = D_f = 0, \beta \to \infty, m = 1, \Pr = Le = 10, \gamma = \pi / 2.$

Nb	Nt	Rafique *et al.,* [13]		HAM	
		$-\theta'(0)$	$-\phi'(0)$	$-\theta'(0)$	$-\phi'(0)$
0.1	0.1	0.9524	2.1294	0.952428	2.129471
0.2	0.2	0.3654	2.5152	0.365436	2.515266
0.3	0.3	0.1355	2.6088	0.135545	2.608814

Table 3
Assessment of $-\theta'(0)$ for different estimates of $\Pr$ in the absence of remaining parameters

$\Pr$	Srinivasulu and Bandari [29]	HAM
0.2	0.196549	0.196552
0.7	0.454442	0.454449
2.0	0.911340	0.911358

5. Results and Discussion

In this section, we describe graphical and tabular perspectives of the characteristics of system boundaries, including flow, temperature, concentration, skin friction, and the Nusselt and Shewhart numbers. The figures are created by changing the quantity of a bound within a defined range to create new ones, while others, like the first images, are kept permanently in place.

$$\beta = 1.0, M = m = 0.5, \lambda = R = Sr = D_f = 0.1, \delta = 0.9, \Pr = Le = 2.0, Nb = Nt = \gamma = 0.2, \Omega = \pi / 4.$$

Figure 3 portrays the impact of magnetic parameter M on the flow fields for different values of M. An electrically conducting fluid in the presence of a magnetic field produces a force that resists the flow, causing the velocity profiles to decrease and the temperature and concentration profiles to increase. On the other hand, the velocity profile slows down for large values of the non-linear stretching parameter m, shown in Figure 4. Physically, the momentum boundary layer thickness reduces for higher values of m.

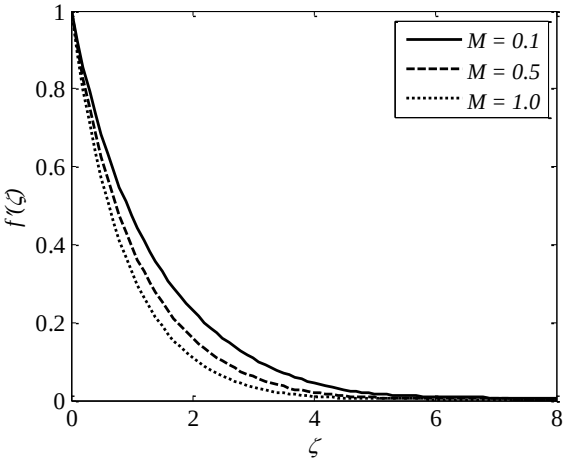

Fig. 3. Variation in $f'(\zeta)$ with M

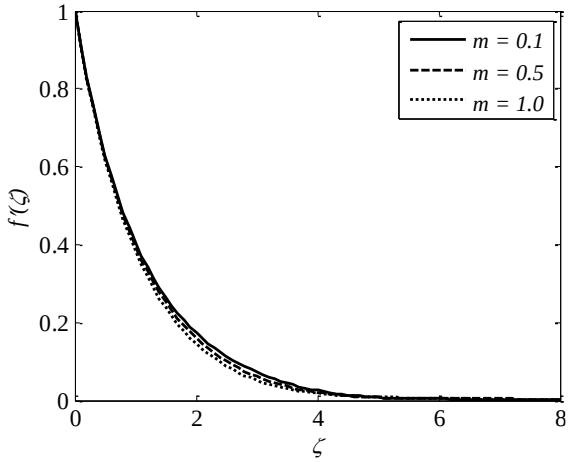

Fig. 4. Variation in $f'(\zeta)$ with m

The impact of the buoyancy parameter is shown in Figure 5. It is observed that the velocity profile increases as the buoyancy parameter increases. This is because the buoyancy effect increases the strength of the fluid flow, which enhances the boundary layer thickness and velocity. Figure 6 indicates that the velocity outline increases by enhancing the solutal buoyancy factor. Physically, the buoyancy parameter reduces the viscous forces whereby the velocity upturns.

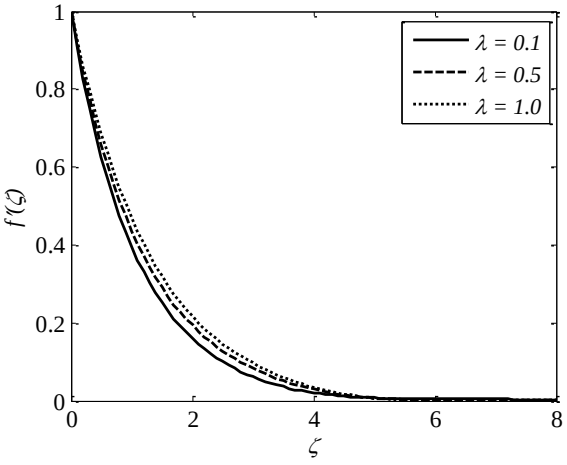

Fig. 5. Variation in $f'(\zeta)$ with λ

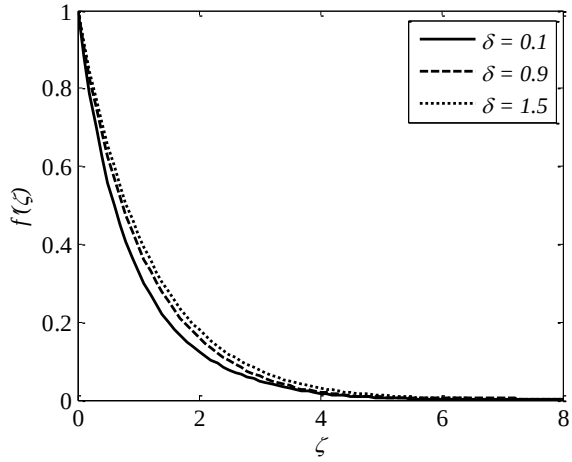

Fig. 6. Variation in $f'(\zeta)$ with δ

The velocity field and inclination parameter correspond to an inverse relation drawn in Figure 7. Physically, by considering $\Omega = 0$, the gravitational force reaches its maximum value. On the contrary, in the case of $\Omega = 90^0$, the sheet will be in horizontal position, and that is why the power of the bouncy forces declines which is the reason behind the reduction in the velocity profile.

The effect of the Casson parameter on the velocity parameter is presented in Figure 8. It is observed that for large values of the Casson parameter, the velocity profile decreases. The reason

behind this behavior is that by increasing the values of the Casson parameter, β increases the fluid viscosity i.e., reducing the yield stress. Therefore, the momentum boundary layer thickness reduces.

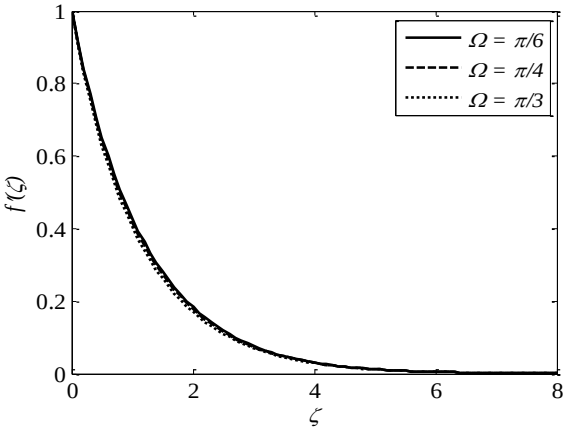

Fig. 7. Variation in $f'(\zeta)$ with Ω

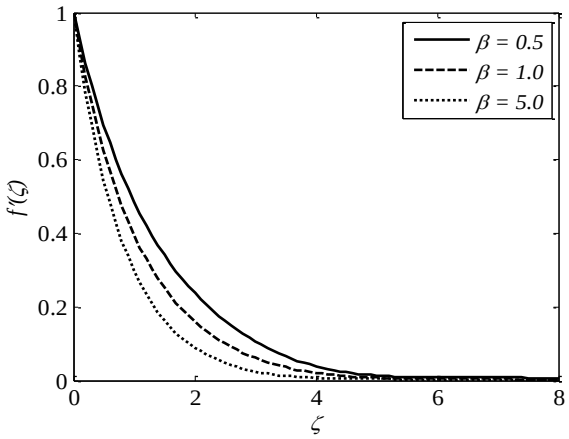

Fig. 8. Variation in $f'(\zeta)$ with β

Figure 9 and Figure 10 show how the Brownian motion factor Nb modifies temperature and concentration curves. The wider range of boosts nanoparticle kinetic energy, allowing more particles to transition beyond the surface, resulting in higher temperatures but lessening concentration.

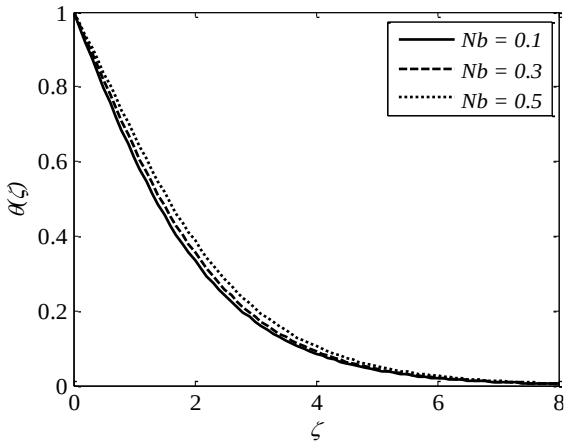

Fig. 9. Variation in $\theta(\zeta)$ with *Nb*

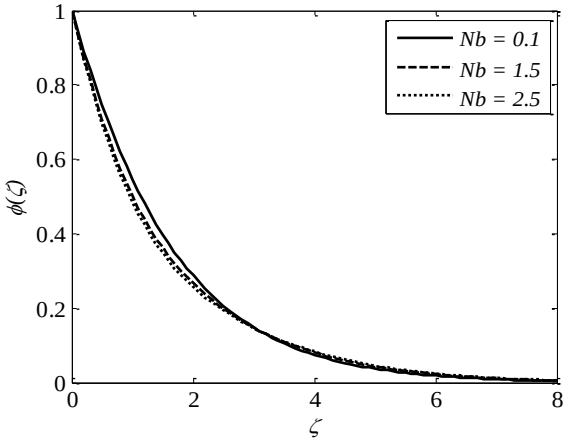

Fig. 10. Variation in $\phi(\zeta)$ with *Nb*

From Figure 11, it can be noticed that the fluid temperature increases by increasing the thermophoresis parameter Nt. This is due to the fact that heated particles are drawn away from hot surfaces and toward colder areas by the thermophoresis force, causing an increase in the fluid temperature inside the boundary layer. It should be mentioned that the thermal conductivity increases with increasing Nt. This is the major reason that leads to the higher concentrations, as presented in Figure 12.

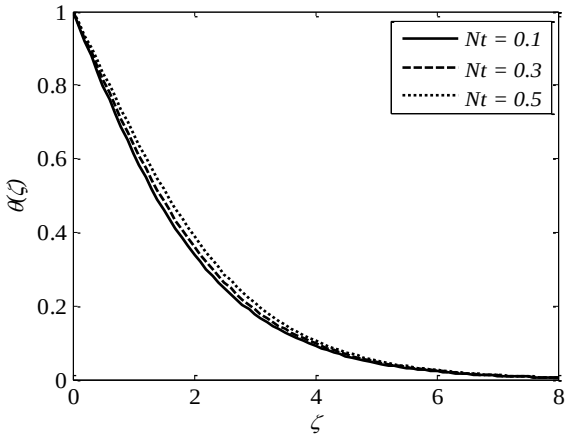

Fig. 11. Variation in $\theta(\zeta)$ with *Nt*

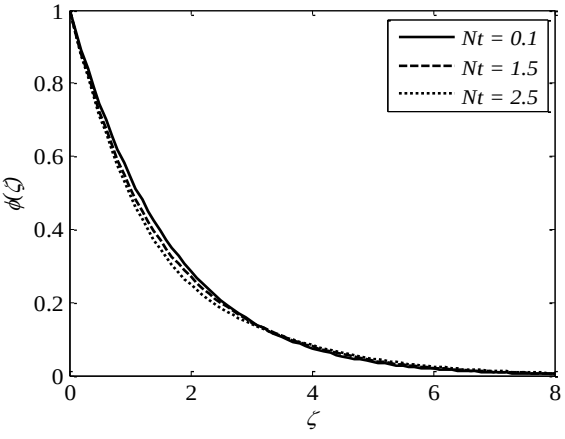

Fig. 12. Variation in $\phi(\zeta)$ with *Nt*

Figure 13 shows that the temperature profile becomes large for larger values in Dufour parameter D_f. This can be justified as an increase in the Dufour parameter, causing an increase in the concentration gradient, resulting in a mass diffusion taking place more rapidly. In this way, the rate of energy transfer related to the particles becomes higher. That is why the temperature profiles enhance. The impact of the Soret number on the concentration profile is observed similar to the impact of the Dufour number on the temperature profile. As parameter Sr increases, the concentration profile increases as displayed in Figure 14.

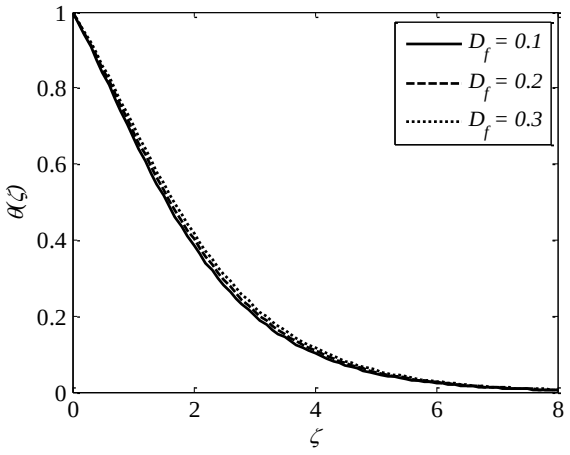

Fig. 13. Variation in $\theta(\zeta)$ with D_f

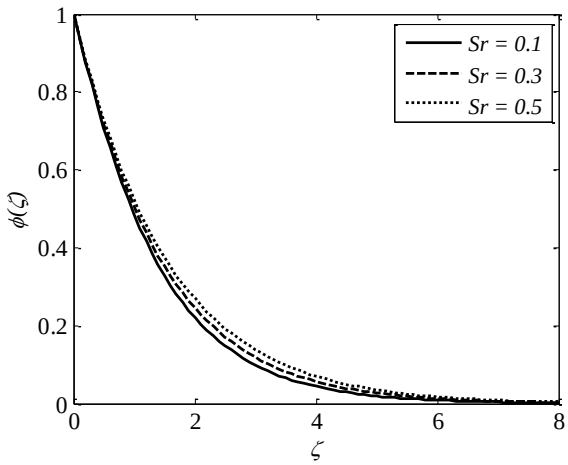

Fig. 14. Variation in $\phi(\zeta)$ with *Sr*

The influence of Prandtl number $\Pr$ on temperature and concentration profiles for various values of $\Pr$ are reported in Figure 15 and Figure 16. $\Pr$ is the ratio of kinematic viscosity to the thermal diffusivity of the fluid. For larger quantities of $\Pr$, have less thermal diffusion. Hence temperature and concentration curves decrease with enhances in $\Pr$.

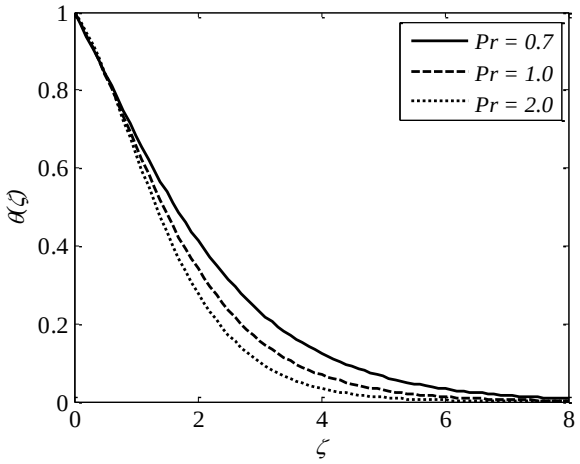

Fig. 15. Variation in $\theta(\zeta)$ with *Pr*

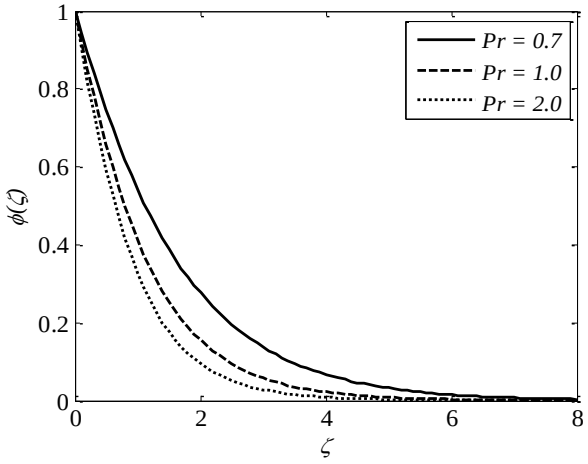

Fig. 16. Variation in $\phi(\zeta)$ with *Pr*

The effect of radiation parameter R on temperature is displayed in Figure 17. It is noticed that the temperature increases with the increase of R. This is due to the fact that the thermal boundary layer thickness increases with the increase of radiation parameter.

Figure 18 shows the concentration profile for various estimates of Lewis Number Le. Concentration profile diminishes with gain in Le. Le is dependent on the Brownian diffusion coefficient. The larger values of Le leads to weaker Brownian diffusion coefficient. Thus, concentration profile diminishes with increase in Le.

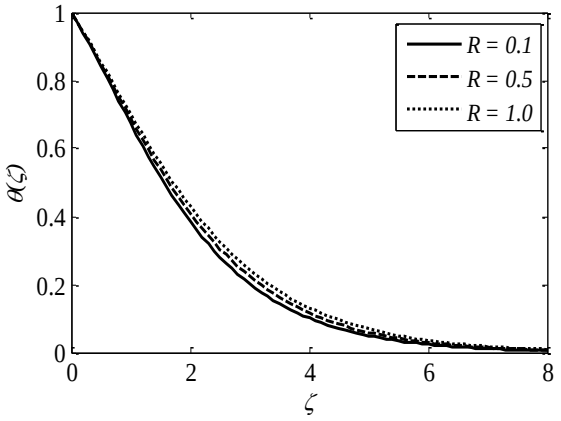

Fig. 17. Variation in $\phi(\zeta)$ with *R*

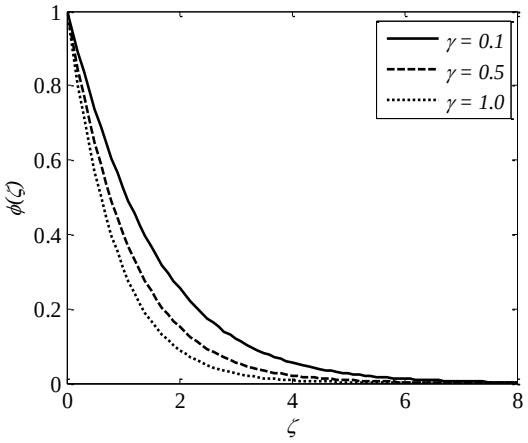

Fig. 18. Variation in $\phi(\zeta)$ with Le

The effect of chemical reaction γ on the resulting concentration profile is depicted in Figure 19. There is a decreasing concentration profile observed as the value of the chemical parameter increases. This happens because the presence of a destructive chemical reduces the thickness of the solutal boundary layer and increases the mass transfer rates. Development in the inclination parameter reduces the skin friction factor but has the reverse effect on the Nusselt and Sherwood numbers. This is shown in Figure 20 to Figure 22.

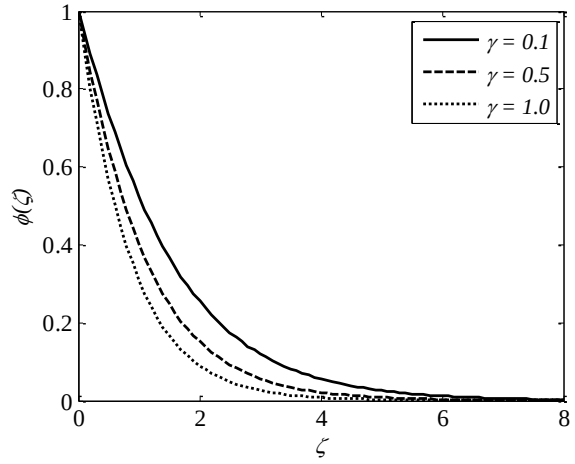

Fig. 19. Variation in $\phi(\zeta)$ with γ

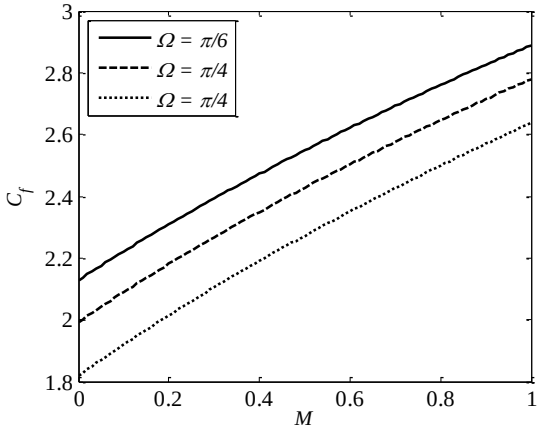

Fig. 20. Variation in C_f with Ω and *M*

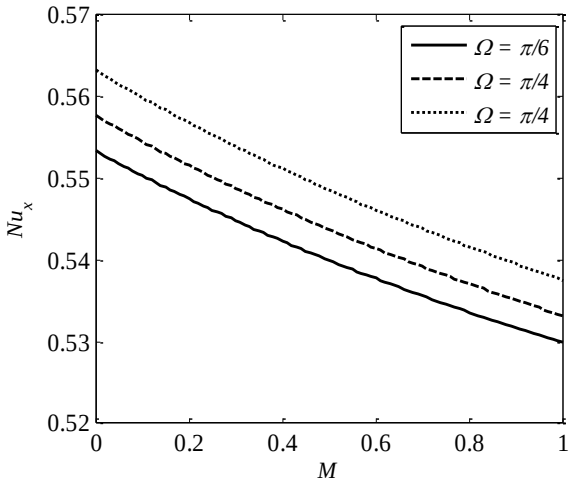

Fig. 21. Variation in Nu_x with Ω and *M*

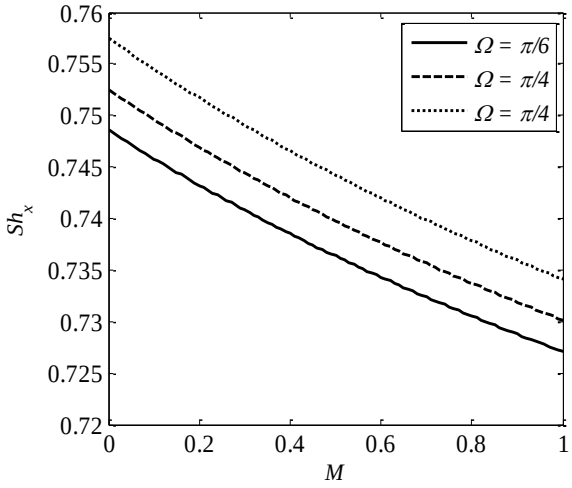

Fig. 22. Variation in Sh_x with Ω and *M*

Figure 23 depicts a comparison of velocity profiles using HAM and numerical findings (NDSolve function in Mathematica) and indicates that the results are comparable across a range of different value of M.

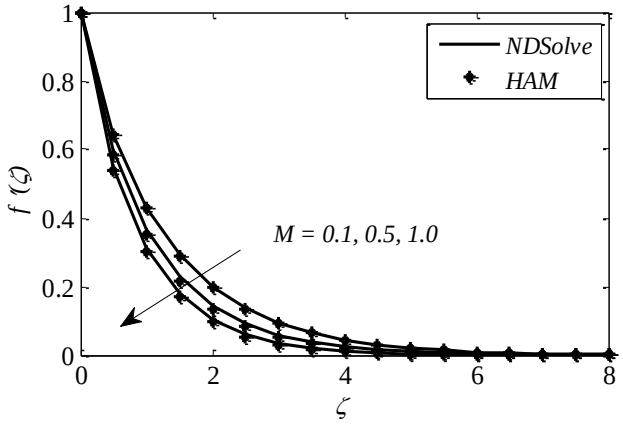

Fig. 23. Comparison of $f'(\zeta)$ for NDSolve and HAM with M

6. Conclusion

In this article, the effects of a Casson nanofluid boundary layer flow over an inclined expanding surface with Soret-Dufour chemical reaction are investigated. The important results are the following:

i. The velocity profile decreases as the inclination parameter increases. An increase in the Casson fluid parameter decreases the velocity profile.
ii. Improving the buoyancy and solutal buoyancy parameters cause an enhancement in the velocity profile.
iii. Thermal radiation boosts temperature field.
iv. Temperature profile upturns when increasing the radiation factor. Dufour effect causes the enhancement in the temperature profile.
v. Mass diffusion and energy of the fluid upturns by enhancing the Brownian motion factor. The thermophoresis factor increases the temperature profile and decreases the concentration profile.
vi. The boundary layer viscosity decreases against Lewis number which relates to a drop in the concentration profile.
vii. Skin friction coefficient decreases with increasing values inclination parameter. But Nusselt number and Sherwood numbers decrease with the increasing values of inclination parameter.

Several scientific and practical applications involving electric fluids are expected to build on the groundwork laid by the present research of flow physics over an exponential stretching regime. The findings may have implications for understanding the migration of subsurface water and the efficacy of various filtration and purification techniques, as well as the flow of oil and gas through a reservoir in an oil or gas field. Finding a solution to this issue may have far-reaching implications, including improvements to heat shifter designs, glass fibre outlining, and nuclear engineering's use of the findings in combination with reactor cooling.

References

[1] Choi, S. US, and Jeffrey A. Eastman. *Enhancing thermal conductivity of fluids with nanoparticles*. No. ANL/MSD/CP-84938; CONF-951135-29. Argonne National Lab.(ANL), Argonne, IL (United States), 1995.
[2] Nakhchi, M. E., and J. A. Esfahani. "Numerical investigation of turbulent Cu-water nanofluid in heat exchanger tube equipped with perforated conical rings." *Advanced Powder Technology* 30, no. 7 (2019): 1338-1347. https://doi.org/10.1016/j.apt.2019.04.009
[3] Ambreen, Tehmina, Arslan Saleem, and Cheol Woo Park. "Numerical analysis of the heat transfer and fluid flow characteristics of a nanofluid-cooled micropin-fin heat sink using the Eulerian-Lagrangian approach." *Powder Technology* 345 (2019): 509-520. https://doi.org/10.1016/j.powtec.2019.01.042
[4] Borah, Abhijit, Manash Protim Boruah, and Sukumar Pati. "Conjugate heat transfer in a duct using nanofluid by two-phase Eulerian-Lagrangian method: effect of non-uniform heating." *Powder Technology* 346 (2019): 180-192. https://doi.org/10.1016/j.powtec.2019.01.059
[5] Javaherdeh, Kourosh, Habib Karimi, and Abbas Khojasteh. "Numerical study of heat transfer enhancement of non-Newtonian nanofluid in porous blocks in a channel partially." *Powder Technology* 383 (2021): 270-279. https://doi.org/10.1016/j.powtec.2021.01.033
[6] Waqas, Hassan, Sumeira Yasmin, Taseer Muhammad, and Muhammad Imran. "Flow and heat transfer of nanofluid over a permeable cylinder with nonlinear thermal radiation." *Journal of Materials Research and Technology* 14 (2021): 2579-2585. https://doi.org/10.1016/j.jmrt.2021.07.030
[7] Jha, Basant K., and Babatunde Aina. "Magnetohydrodynamic natural convection flow in a vertical micro-porous-channel in the presence of induced magnetic field." *Communications in Nonlinear Science and Numerical Simulation* 64 (2018): 14-34. https://doi.org/10.1016/j.cnsns.2018.04.004

[8] Elsaid, Essam M., and Mohamed S. Abdel-wahed. "MHD mixed convection Ferro Fe_3O_4/Cu-hybrid-nanofluid runs in a vertical channel." *Chinese Journal of Physics* 76 (2022): 269-282. https://doi.org/10.1016/j.cjph.2021.12.016
[9] Iqbal, Z., N. S. Akbar, Ehtsham Azhar, and E. N. Maraj. "Performance of hybrid nanofluid (Cu-CuO/water) on MHD rotating transport in oscillating vertical channel inspired by Hall current and thermal radiation." *Alexandria Engineering Journal* 57, no. 3 (2018): 1943-1954. https://doi.org/10.1016/j.aej.2017.03.047
[10] Alharbi, Sayer Obaid. "Impact of hybrid nanoparticles on transport mechanism in magnetohydrodynamic fluid flow exposed to induced magnetic field." *Ain Shams Engineering Journal* 12, no. 1 (2021): 995-1000. https://doi.org/10.1016/j.asej.2020.04.013
[11] Sharma, Anuj Kumar, Arun Kumar Tiwari, and Amit Rai Dixit. "Rheological behaviour of nanofluids: A review." *Renewable and Sustainable Energy Reviews* 53 (2016): 779-791. https://doi.org/10.1016/j.rser.2015.09.033
[12] Mintsa, Honorine Angue, Gilles Roy, Cong Tam Nguyen, and Dominique Doucet. "New temperature dependent thermal conductivity data for water-based nanofluids." *International Journal of Thermal Sciences* 48, no. 2 (2009): 363-371. https://doi.org/10.1016/j.ijthermalsci.2008.03.009
[13] Rafique, Khuram, Muhammad Imran Anwar, Masnita Misiran, Ilyas Khan, S. O. Alharbi, Phatiphat Thounthong, and K. S. Nisar. "Numerical solution of casson nanofluid flow over a non-linear inclined surface with soret and dufour effects by keller-box method." *Frontiers in Physics* 7 (2019): 139. https://doi.org/10.3389/fphy.2019.00139
[14] Mukhopadhyay, Swati. "Casson fluid flow and heat transfer over a nonlinearly stretching surface." *Chinese Physics B* 22, no. 7 (2013): 074701. https://doi.org/10.1088/1674-1056/22/7/074701
[15] Mustafa, M., and Junaid Ahmad Khan. "Model for flow of Casson nanofluid past a non-linearly stretching sheet considering magnetic field effects." *AIP Advances* 5, no. 7 (2015). https://doi.org/10.1063/1.4927449
[16] Gnanaprasanna, K., and Abhishek Kumar Singh. "A numerical approach of forced convection of Casson nanofluid flow over a vertical plate with varying viscosity and thermal conductivity." *Heat Transfer* 51, no. 7 (2022): 6782-6800. https://doi.org/10.1002/htj.22623
[17] Hayat, T., S. A. Shehzad, and A. Alsaedi. "Soret and Dufour effects on magnetohydrodynamic (MHD) flow of Casson fluid." *Applied Mathematics and Mechanics* 33 (2012): 1301-1312. https://doi.org/10.1007/s10483-012-1623-6
[18] Ashgar, Adnan, and Teh Yuan Ying. "Three dimensional MHD hybrid nanofluid Flow with rotating stretching/shrinking sheet and Joule heating." *CFD Letters* 13, no. 8 (2021): 1-19. https://doi.org/10.37934/cfdl.13.8.119
[19] Rusdi, Nadia Diana Mohd, Siti Suzilliana Putri Mohamed Isa, Norihan Md Arifin, and Norfifah Bachok. "Thermal Radiation in Nanofluid Penetrable Flow Bounded with Partial Slip Condition." *CFD Letters* 13, no. 8 (2021): 32-44. https://doi.org/10.37934/cfdl.13.8.3244
[20] Bakar, Shahirah Abu, Norihan Md Arifin, and Ioan Pop. "Stability Analysis on Mixed Convection Nanofluid Flow in a Permeable Porous Medium with Radiation and Internal Heat Generation." *Journal of Advanced Research in Micro and Nano Engineering* 13, no. 1 (2023): 1-17. https://doi.org/10.37934/armne.13.1.117
[21] Ramanuja, Mani, J. Kavitha, A. Sudhakar, A. Ajay Babu, Hari Kamala Sree, and K. Ramesh Babu. "Effect of Chemically Reactive Nanofluid Flowing Across Horizontal Cylinder: Numerical Solution." *Journal of Advanced Research in Numerical Heat Transfer* 12, no. 1 (2023): 1-17.
[22] Zangooee, M. R., Kh Hosseinzadeh, and Davood Domiri Ganji. "Hydrothermal analysis of Ag and CuO hybrid NPs suspended in mixture of water 20%+ EG 80% between two concentric cylinders." *Case Studies in Thermal Engineering* 50 (2023): 103398. https://doi.org/10.1016/j.csite.2023.103398
[23] Alipour, Navid, Bahram Jafari, and Kh Hosseinzadeh. "Optimization of wavy trapezoidal porous cavity containing mixture hybrid nanofluid (water/ethylene glycol Go-Al_2O_3) by response surface method." *Scientific Reports* 13, no. 1 (2023): 1635. https://doi.org/10.1038/s41598-023-28916-2
[24] Gulzar, M. Mudassar, Anmol Aslam, M. Waqas, M. Asif Javed, and Kh Hosseinzadeh. "A nonlinear mathematical analysis for magneto-hyperbolic-tangent liquid featuring simultaneous aspects of magnetic field, heat source and thermal stratification." *Applied Nanoscience* 10 (2020): 4513-4518. https://doi.org/10.1007/s13204-020-01483-y
[25] Prasad, P. Durga, RVMSS Kiran Kumar, and S. V. K. Varma. "Heat and mass transfer analysis for the MHD flow of nanofluid with radiation absorption." *Ain Shams Engineering Journal* 9, no. 4 (2018): 801-813. https://doi.org/10.1016/j.asej.2016.04.016
[26] Akbar, Muhammad Zubair, Muhammad Ashraf, Muhammad Farooq Iqbal, and Kashif Ali. "Heat and mass transfer analysis of unsteady MHD nanofluid flow through a channel with moving porous walls and medium." *AIP Advances* 6, no. 4 (2016). https://doi.org/10.1063/1.4945440
[27] Nadeem, Sohail, and Changhoon Lee. "Boundary layer flow of nanofluid over an exponentially stretching surface." *Nanoscale Research Letters* 7 (2012): 1-6. https://doi.org/10.1186/1556-276X-7-94
[28] Kay, E. D., Stephen Hibberd, and Henry Power. "A multi-layer integral model for locally-heated thin film flow." *Journal of Computational Physics* 336 (2017): 51-68. https://doi.org/10.1016/j.jcp.2017.01.066

[29] Srinivasulu, T., and Shankar Bandari. "MHD, Nonlinear thermal radiation and non-uniform heat source/sink effect on Williamson nanofluid over an inclined stretching sheet." *Malaya Journal of Matematik (MJM)* 8, no. 3 (2020): 1337-1345. https://doi.org/10.26637/MJM0803/0106

[30] Ali, Mohammad, Md Abdul Alim, and Mohammad Shah Alam. "Heat transfer boundary layer flow past an inclined stretching sheet in the presence of magnetic field." *International Journal of Advancements in Research & Technology* 3, no. 5 (2014): 34-40.

[31] Ramesh, G. K., B. J. Gireesha, and C. S. Bagewadi. "Heat transfer in MHD dusty boundary layer flow over an inclined stretching sheet with non-uniform heat source/sink." *Advances in Mathematical Physics* 2012 (2012). https://doi.org/10.1155/2012/657805

[32] Nandeppanavar, Mahantesh M., T. Srinivasulu, and Shanker Bandari. "MHD flow and heat transfer analysis of Newtonian and non-Newtonian nanofluids due to an inclined stretching surface." *Multidiscipline Modeling in Materials and Structures* 16, no. 1 (2020): 134-155. https://doi.org/10.1108/MMMS-11-2018-0192

[33] Rafique, Khuram, and Hammad Alotaibi. "Numerical simulation of Williamson nanofluid flow over an inclined surface: Keller box analysis." *Applied Sciences* 11, no. 23 (2021): 11523. https://doi.org/10.3390/app112311523

[34] Shah, Sajid, Shahzada M. Atif, and Abid Kamran. "Radiation and slip effects on MHD Maxwell nanofluid flow over an inclined surface with chemical reaction." *Heat Transfer* 50, no. 4 (2021): 4062-4085. https://doi.org/10.1002/htj.22064

[35] Saeed, Anwar, Poom Kumam, Saleem Nasir, Taza Gul, and Wiyada Kumam. "Non-linear convective flow of the thin film nanofluid over an inclined stretching surface." *Scientific Reports* 11, no. 1 (2021): 18410. https://doi.org/10.1038/s41598-021-97576-x

[36] Liao, Shijun. *Homotopy analysis method in nonlinear differential equations*. Beijing: Higher Education Press, 2012. https://doi.org/10.1007/978-3-642-25132-0

[37] Nadeem, Sohail, Rizwan Ul Haq, and Noreen Sher Akbar. "MHD three-dimensional boundary layer flow of Casson nanofluid past a linearly stretching sheet with convective boundary condition." *IEEE Transactions on Nanotechnology* 13, no. 1 (2013): 109-115. https://doi.org/10.1109/TNANO.2013.2293735

[38] Ibrahim, S. M., G. Lorenzini, P. Vijaya Kumar, and C. S. K. Raju. "Influence of chemical reaction and heat source on dissipative MHD mixed convection flow of a Casson nanofluid over a nonlinear permeable stretching sheet." *International Journal of Heat and Mass Transfer* 111 (2017): 346-355. https://doi.org/10.1016/j.ijheatmasstransfer.2017.03.097

[39] Ibrahim, S. M., P. V. Kumar, G. Lorenzini, and E. Lorenzini. "Influence of Joule heating and heat source on radiative MHD flow over a stretching porous sheet with power-law heat flux." *Journal of Engineering Thermophysics* 28 (2019): 332-344. https://doi.org/10.1134/S1810232819030044

[40] Hayat, T., S. A. Shehzad, and A. Alsaedi. "Soret and Dufour effects on magnetohydrodynamic (MHD) flow of Casson fluid." *Applied Mathematics and Mechanics* 33 (2012): 1301-1312. https://doi.org/10.1007/s10483-012-1623-6